



Functional periodontal regeneration using biomineralized extracellular matrix/stem cell microspheroids

Sheng-Jie Cui^{a,1}, Yu Fu^{b,1}, Min Yu^a, Lei Zhang^c, Wen-Yan Zhao^c, Ting Zhang^a, Li-Xin Qiu^b, Yan Gu^a, Yan-Heng Zhou^a, Yan Liu^{a,*}

^a Laboratory of Biomimetic Nanomaterials, Department of Orthodontics, Peking University School and Hospital of Stomatology & National Center of Stomatology & National Clinical Research Center for Oral Diseases & National Engineering Laboratory for Digital and Material Technology of Stomatology & Beijing Key Laboratory of Digital Stomatology & Research Center of Engineering and Technology for Computerized Dentistry Ministry of Health & NMPA Key Laboratory for Dental Materials, Beijing 100081, China

^b Fourth Clinical Division, Peking University School and Hospital of Stomatology & National Center of Stomatology & National Clinical Research Center for Oral Diseases & National Engineering Laboratory for Digital and Material Technology of Stomatology & Beijing Key Laboratory of Digital Stomatology & Research Center of Engineering and Technology for Computerized Dentistry Ministry of Health & NMPA Key Laboratory for Dental Materials, Beijing 100081, China

^c Yinchuan Stomatology Hospital, Yinchuan, Ningxia 750002, China

ARTICLE INFO

Keywords:

Periodontal regeneration
Biomineralization
Cell microspheroids
Dental pulp stem cells
TGF- β 1

ABSTRACT

Engineering complete periodontal tissue regeneration remains a considerable clinical challenge because the native periodontium is composed of hard mineralized and soft unmineralized tissues. Stem cell therapies that use endogenous extracellular matrix (ECM) have the potential for structural and functional periodontal regeneration. Here, mineralized ECM/dental pulp stem cell microspheroids (MMCMs) mimicking native mesenchymal microspheroid precursors were developed, and showed an enhanced Young's modulus ranging from 0.4 GPa to 1.9 GPa. Furthermore, biomineralization promoted cell viability, inhibited cell apoptosis, and enhanced ECM secretion and osteogenic differentiation potential in dental pulp stem cells. After implantation in the full periodontal defect, MMCMs regenerated complete periodontium with native-like hierarchically organized periodontal ligament collagen fibers inserted into the newly formed alveolar bone and cementum; they also recruited CD90⁺CD73⁺ host mesenchymal stem cells. Mechanistically, MMCMs promoted functional periodontal regeneration through activation of the transforming growth factor beta 1 (TGF- β 1)/Smad3 signaling pathway. Inhibition of TGF- β 1 signaling pathway significantly impaired osteogenic potential and matrix secretion of MMCMs, while exogenous TGF- β 1 treatment enhanced the osteogenesis and periodontal regeneration outcomes of MMCMs. These results indicate the promising application of MMCMs in complex tissue regeneration.

1. Introduction

Periodontal defects, including resorption of hard tissue (e.g., alveolar bone and cementum) and destruction of soft tissue (e.g., periodontal ligament), are the main causes of early tooth loss [1]. The occurrence of periodontal defects involves local immune and inflammatory responses, abnormal alveolar bone metabolism, and reduced numbers and impaired functions of autologous stem cells. Complete, functional periodontal tissue regeneration requires reconstitution of the adjacent

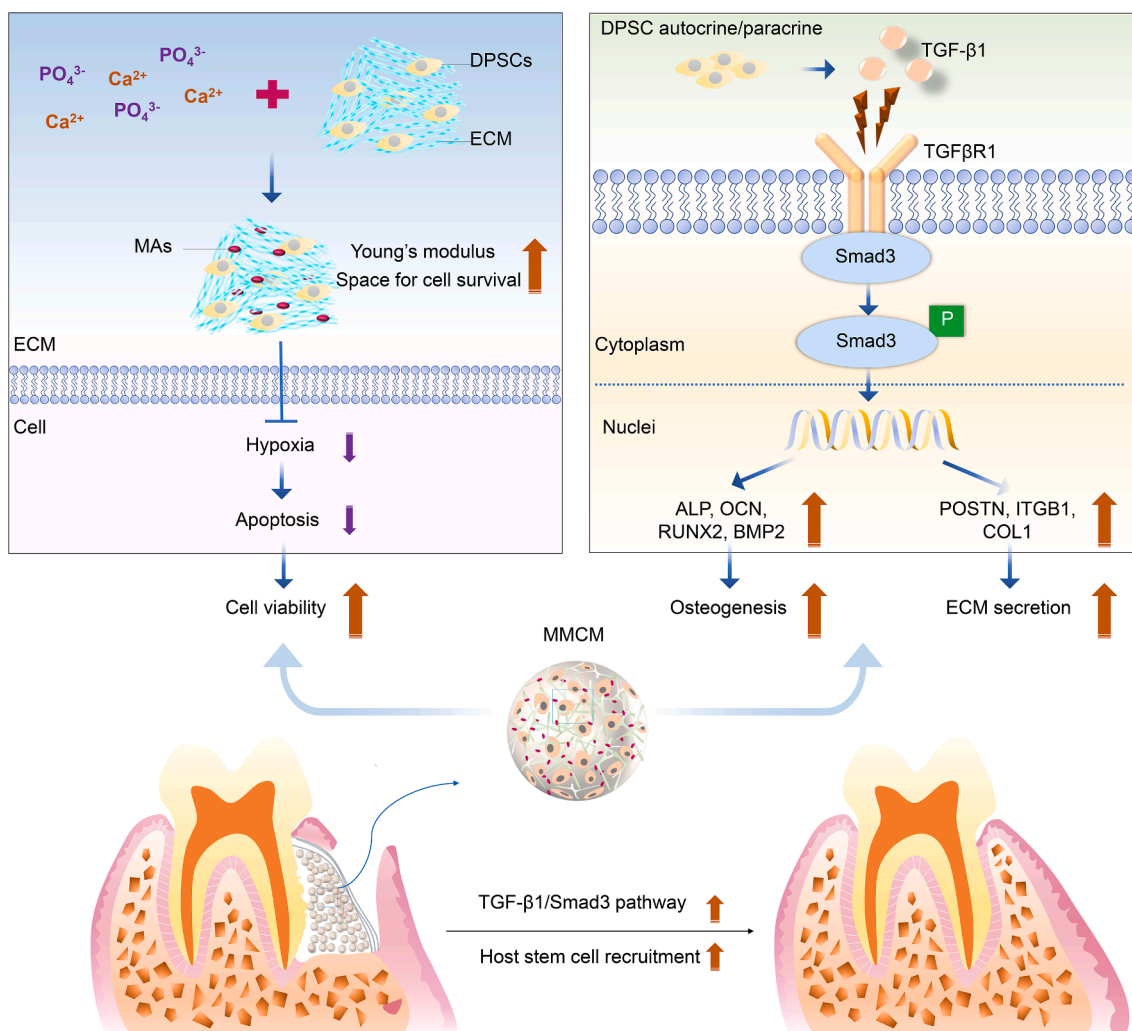
resorbed alveolar bone, as well as the formation of periodontal ligament fibers inserted into the newly formed cementum and alveolar bone. Existing periodontal therapies, such as guided tissue regeneration, periodontal flap operation, and the administration of drugs or bioactive molecules can control inflammation, clean necrotic tissues, and partially limit the migration of gingival epithelium, but the structural and functional regeneration of periodontium remains challenging [2].

Recently, tissue engineering strategies combining bone grafting materials and mesenchymal stem cells (MSCs) provide a promising

* Corresponding author at: Prof. Yan Liu, Laboratory of Biomimetic Nanomaterials, Department of Orthodontics, Peking University School and Hospital of Stomatology & National Center of Stomatology & National Clinical Research Center for Oral Diseases & National Engineering Laboratory for Digital and Material Technology of Stomatology & Beijing Key Laboratory of Digital Stomatology & Research Center of Engineering and Technology for Computerized Dentistry Ministry of Health & NMPA Key Laboratory for Dental Materials, No.22 Zhongguancun South Avenue, Beijing 100081, China.

E-mail address: orthoyan@bjmu.edu.cn (Y. Liu).

¹ These authors contributed equally to this work.



Scheme 1. Schematic illustration showing structural and functional periodontal tissue regeneration by biomineralized ECM/DPSC microspheroids via the TGF- β 1/Smad3 signaling pathway. Biomineralization of microspheroids modulates multiple cellular processes of DPSCs, including viability, osteogenesis and ECM secretion *in vitro*; and promotes structural and functional periodontal tissue regeneration and host stem cell recruitment *in vivo*.

method to achieve complex tissue regeneration [3]. Park *et al.* engineered bone-ligament complex structure using poly- ϵ -caprolactone fiber-guiding scaffolds with periodontal ligament cell transplantation [4]. Liu *et al.* reported a specific “cell perfusion” technique that loaded human periodontal ligament stem cells on poly[lactic-co-(glycolic acid)] hybrid porous microspheres for periodontitis treatment [5]. However, the use of exogenous scaffold is inevitably associated with various problems, including immunorejection, poor degradation rate and incompatibility between the exogenous scaffold and the host [6]. Therefore, a scaffold-free MSC carrier would be an excellent alternative to address these problems.

The self-secreted extracellular matrix (ECM) by MSCs is a complex structural network consisting of primarily fibrous proteins, proteoglycans and glycosaminoglycans, and plays a vital role in MSC recognition of physical and biochemical cues [7]. It has been shown that cell-ECM reciprocal communications influence MSC stemness and cell fate [8]. Further, cell-secreted ECM reportedly maintains MSC multipotency during *in vitro* expansion and rejuvenates the cell functions of aging MSCs [9]. However, conventional two-dimensional cell culture results in altered cell shape (e.g., cell flattening and cytoskeletal remodeling), which can eventually affect cellular perception of the external microenvironment and cause changes in related gene expression [10]. Compared with traditional two-dimensionally cultured cells, three-dimensionally cultured cell aggregates (e.g., cell sheets and

microspheroids) maintain microenvironmental conditions similar to the conditions they encounter *in vivo*, which thus promote active ECM synthesis [11]. Zhang *et al.* showed complex periodontium-like formation by combination of MSC cell sheets and ceramic bovine bone in nude mice [12]. Although cell sheets showed promising periodontal regenerative effects, they still rely on the combination of exogenous scaffolds or multiple derived MSCs or specific gene transfection to enhance the therapeutic capacity [13,14]. Compared with cell sheets fabricated through complicated procedures, cell microspheroids could spontaneously form three-dimensional (3D) endogenous scaffolds. However, the application of cell microspheroids still have some problems, such as the impaired cell maturation and cell viability due to the enlarged spheroid size and consequent hypoxia in the spheroid core [15].

An ideal biomaterial for periodontal regeneration must provide sufficient mechanical strength to maintain defect space and support MSC proliferation and differentiation. In the present study, we constructed 3D osteoinductive microspheroids composed of dental pulp stem cells (DPSCs) with multilineage differentiation potential and mineralized ECM as an endogenous scaffold. Mineralization of the ECM enhanced the mechanical strength of cell microspheroids, prevented cell hypoxia and apoptosis, and improved cell viability; this effect was most evident in the spheroid core area. Moreover, biomimetic mineralization activated the transforming growth factor beta 1 (TGF- β 1)/Smad3 signaling pathway, then upregulated the ECM synthesis and osteogenesis abilities. By

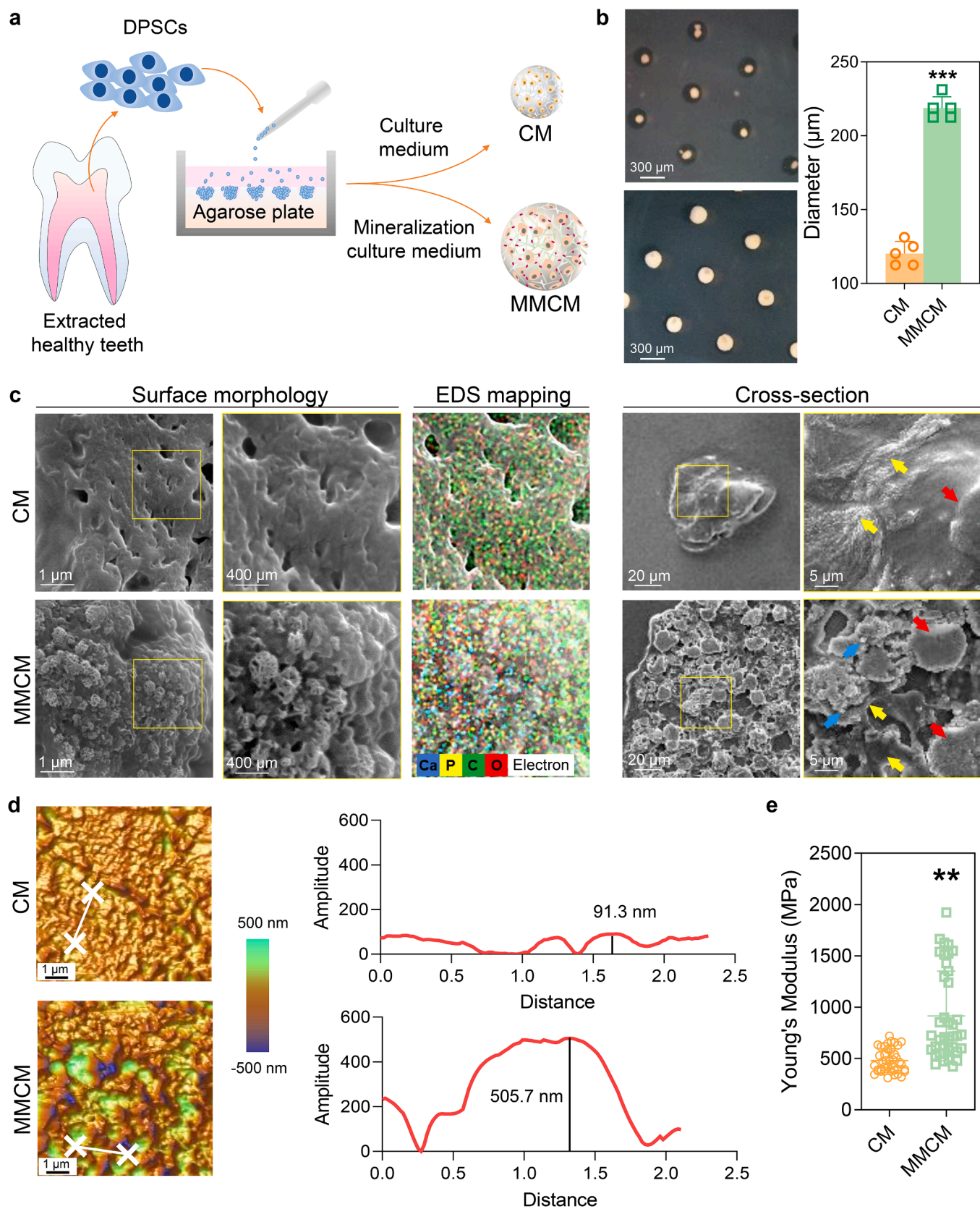


Fig. 1. Fabrication and characterization of 3D mineralized cell microspheroids after 7 days cultivation. (a) Scheme showing fabrication of CMs and MMCMs. (b) Gross morphology and diameter of CMs and MMCMs ($n = 5$, Student's t -test). (c) Ultrastructure and composition of CMs and MMCMs. Yellow arrows: ECM collagen filaments; Blue arrows: MAs; Red arrows: DPSCs. (d) AFM height mapping images and corresponding amplitude spectrums of CMs and MMCMs. (e) AFM Young's modulus of CMs and MMCMs ($n = 40$, Kolmogorov-Smirnov nonparametric test). **: $P < 0.01$, ***: $P < 0.001$. (For interpretation of the references to colour in this figure legend, the reader is referred to the web version of this article.)

constructing full periodontal defects in a rat model, we showed that mineralized ECM/dental pulp stem cell microspheroids (MMCMs) recruited CD90⁺CD73⁺ host MSCs, then potently induced structural and functional periodontium regeneration with orderly aligned periodontal ligament fibers inserted into the newly formed bone and cementum through activation of the TGF- β 1/Smad3 signaling pathway. Furthermore, blockade of TGF- β 1 significantly impaired matrix secretion and osteogenesis, while exogenous TGF- β 1 treatment improved the periodontal regeneration effect of MMCMs (Scheme 1). Taken together, these observations suggested that MMCMs offer a promising alternative for structural and functional periodontium regeneration.

2. Materials and methods

2.1. Isolation and identification of human DPSCs

Primary human DPSCs were isolated from dental pulps of the extracted healthy premolars or wisdom teeth due to orthodontic treatment. All procedures were approved by the Ethics Committee of Peking University School of Stomatology (No. PKUSSIRB-201951179). The harvested pulp tissues were dissected and digested in 3 mg/ml Type I collagenase (Thermo Fisher Scientific) and 4 mg/ml dispase (Roche) at 37 °C for 1 h as previously described [16]. After passing through a 70- μ m strainer, single-cell suspensions were cultured in of minimum essential Eagle medium- α modification (α -MEM, Hyclone) supplemented with 15% fetal bovine serum (FBS, Hyclone), 2 mM L-glutamine (Thermo Fisher Scientific), and 100 U/ml penicillin/streptomycin (Thermo Fisher Scientific). At 80%-90% confluence, cells were digested with trypsin, centrifuged and resuspended in culture medium as passage 1, and incubated in a humidified atmosphere of 5% CO₂ at 37 °C, with medium changing every 2–3 days.

For flow cytometry analysis, 1×10^6 DPSCs were incubated with fluorescently conjugated antibodies of CD90, CD105, CD146, CD29, CD34 and CD11b or isotype-matched IgG controls at room temperature for 1 h. Stained cells were analyzed with flow cytometer (BD Accuri C6).

To investigate the osteogenic potential, DPSCs at passage 3 were cultured in the osteogenic induction medium when the cells achieved 70%–80% confluency. After 21 days, DPSCs were fixed for alizarin red S staining (Sigma-Aldrich). For adipogenic differentiation, DPSCs at passage 3 were cultured in the adipogenic induction medium for 21 days. Then, cells were fixed and stained with fresh oil red O solution (Sigma-Aldrich).

2.2. Preparation of cell microspheroids

Human DPSCs at passage 4 were seeded in microporous agarose plate (Ryan) with a density of 5×10^3 cells/microwell (Fig. 1a). Two kinds of cell culture media were used as follows: regular medium (α -MEM containing 15% FBS, 2 mM L-glutamine, and 100 U/ml penicillin/streptomycin) was utilized to prepare conventional cell microspheroids (CMs), while mineralization medium (regular medium with 9×10^{-3} M CaCl₂, 4.2×10^{-3} M K₂HPO₄ and 0.2 mg/ml polyaspartic acid) was used to fabricate MMCMs. Cells were cultured in a humidified atmosphere of 5% CO₂ for 1, 3 and 7 days, and the culture medium was changed 24 h after primary seeding and then refreshed every two days. The harvested microspheroids were then selected by 40- μ m cell sieves and those >40 μ m in diameter were collected for the following experiments.

To evaluate the influence of TGF- β 1/Smad3 pathway, the specific inhibitor LY364947 (3 μ M, Selleck) or TGF- β 1 (10 ng/mL, Peprotech) were consistently added into the mineralization culture medium, respectively.

2.3. Characterization of cell microspheroids

Microspheroids were randomly selected from each group. Samples were fixed by 2.5% glutaraldehyde. All the samples were dehydrated in

a graded series of ethanol (30%, 50%, 70%, 80%, 90%, 95%, and 100%), and observed under scanning electron microscopy (SEM) at 15 kV (Hitachi S-4800, Japan). The elemental compositions of CMs and MMCMs were examined through energy dispersive X-ray spectroscopy (EDS) coupled to SEM. For morphological observation by transmission electron microscopy (TEM), samples were fixed with 2.5% glutaraldehyde solution. The samples were embedded in epoxy resin. Before observed by TEM at 80 kV (JEOL, Japan), ultrathin sections (70 nm) were stained with uranyl acetate.

Microspheroids were washed twice with phosphate-buffered saline (PBS), and immediately embedded with Tissue-Tek (Sakura Finetek) to make 20 μ m thick frozen sections. Using the Bruker Icon Atomic force microscopy (AFM) and TAP150A silicon cantilever, the same maximum force value was applied to different samples during the experiment, and the Young's modulus and corresponding adhesive force of the samples in the range of 8 μ m \times 8 μ m were scanned. A 512 \times 512 high-resolution contour map was generated. Data for statistical analysis for AFM was collected from at least three independent samples.

2.4. Cell viability and proliferation

To detect cell viability, CMs and MMCMs were stained with a live/dead assay kit (Thermo Fisher Scientific) according to the manufacturer's protocol and observed with a Zeiss laser scanning confocal microscope LSM 710.

To evaluate the proliferation of cells, samples were incubated in Cell Counting Kit-8 (CCK-8) solution (Dojindo) according to standard procedures (37 °C for 2 h), and the absorbance was read at 450 nm by a microplate reader (Bio-Rad). Each group had eight replicates.

2.5. Assessment of relative gene expression

Quantitative real-time polymerase chain reaction (qPCR) was applied to examine the expression of *B-cell lymphoma-2 (BCL2)*, *BCL2 associated X protein (BAX)*, *periostin (POSTN)*, *integrin β 2 (ITGB2)*, *alkaline phosphatase (ALP)*, *runt-related transcription factor 2 (RUNX2)*, *osteocalcin (OCN)*, *bone morphogenetic protein 2 (BMP2)* and *collagen type I alpha 1 chain (COL1A1)*. *18S RNA* served as the housekeeping gene. Total RNA was extracted by TRIzol reagent (Invitrogen) and synthesis of cDNA was performed using SuperScript® III One-Step RT-PCR System with Platinum® Taq High Fidelity (Invitrogen). qPCR was performed on a 7500HT Fast Real Time PCR machine (Applied Biosystems) using SYBR Green (Invitrogen). The primers designed by primer premier 5.0 software and commercially synthesized were shown in Table S1.

2.6. Assessment of protein expression

Total proteins of cells in CMs and MMCMs were lysed using a protein extraction kit (RIPA Cocktail, Thermo). Equal protein quantities were separated by SDS-PAGE and transferred onto a polyvinylidene difluoride membrane. The membranes were blocked with 5% non-fat milk and 0.1% Tween-20 for 1 h, then incubated with hypoxia-inducible factor 1- α (HIF-1 α), carbonic anhydrase IX (CA IX), ALP (Santa Cruz Biotechnology), OCN, BMP2, TGF- β 1 (Abcam), cleaved Caspase3, p-Smad3, Smad3 (Cell Signaling Technology), COL1 (collagen type I, Proteintech), β -actin (ZSGB-BIO) and GAPDH (glyceraldehyde-3-phosphate dehydrogenase, Affinity) primary antibodies overnight at 4 °C (Table S2). The blots were developed using an HRP-conjugated secondary antibody and enhanced chemiluminescence detection. Quantitative analysis was performed by the ImageLab software. The original images of all Western blotting were displayed in Fig. S5.

2.7. In vivo tests

Eight-week-old male Sprague-Dawley rats were randomly divided into different groups. After intraperitoneal injection of 1%

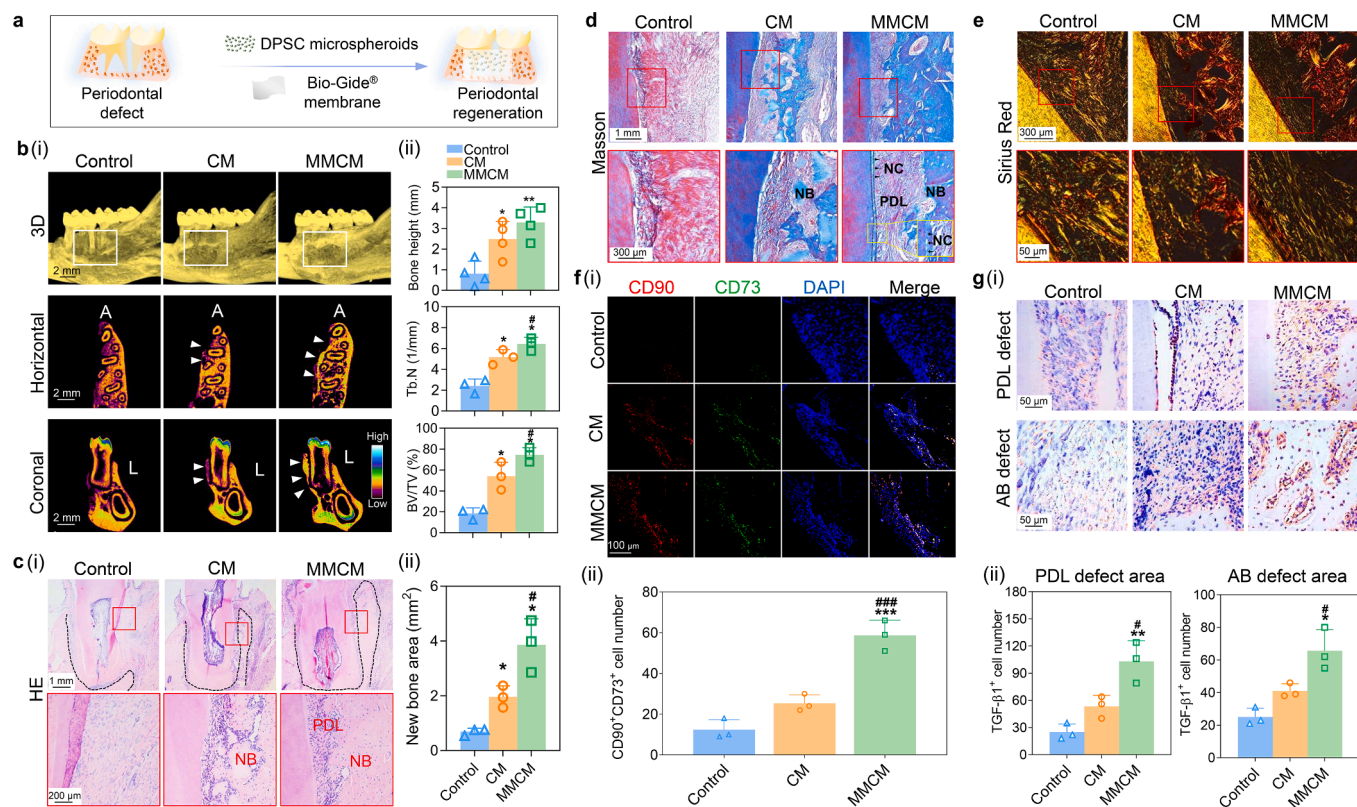


Fig. 3. Complete periodontal tissue regeneration by MMCMs. **(a)** Scheme of surgical procedure for periodontal regeneration. **(b)** (i) Representative micro-CT images (3D, horizontal plane, coronal plane) of periodontal tissues at 4 weeks postoperatively. A: anterior; L: lingual; white arrows: newly formed bone. **(ii)** Semi-quantitative analysis of bone-related parameters including vertical bone height, Tb.N and BV/TV% ($n = 3$ or 4, ANOVA with Tukey's comparison test). *: versus control, #: versus CM. *: $P < 0.05$, **: $P < 0.01$. **(c)** HE staining of coronal sections (i) and semi-quantitative analysis of new bone area (ii) ($n = 3$, ANOVA with Tukey's comparison test). *: versus control, #: versus CM. *: $P < 0.05$, **: versus CM. *: $P < 0.05$, **: versus CM. *: $P < 0.05$, **: $P < 0.01$. NB: new bone; PDL: periodontal ligament; black dotted frame: the boundary of alveolar bone area; red frame: high magnification the defect area. **(d, e)** Masson trichrome and picrosirius red (under polarized light) stainings of coronal sections. NB: new bone; PDL: periodontal ligament; NC: new cementum; red frame: high magnification the defect area. **(f)** Representative images (i) and semi-quantitative analysis (ii) of immunofluorescence staining of CD90 (red) and CD73 (green) ($n = 3$, ANOVA with Tukey's comparison test). CD90⁺CD73⁺ cell number was counted in $400 \mu\text{m} \times 400 \mu\text{m}$ area. *: versus control, #: versus CM. ***: $P < 0.001$. **(g)** Representative images (i) and semi-quantitative analysis (ii) of immunohistochemistry of TGF-β1 ($n = 3$, ANOVA with Tukey's comparison test). Positive cell number was counted in $300 \mu\text{m} \times 300 \mu\text{m}$ area. *: versus control, #: versus CM. *: $P < 0.05$, **: $P < 0.01$. (For interpretation of the references to colour in this figure legend, the reader is referred to the web version of this article.)

incubated with anti-BMP2 (1:200; Abcam), anti-POSTN (1:200; Abcam) and anti-TGF-β1 (1:250; Abcam) antibodies overnight at 4 °C, followed by washing and incubating with horseradish-peroxidase-conjugated secondary antibodies. For immunofluorescence staining, sections or cells were incubated with anti-CD90 (1:200; BD Pharmingen), anti-CD73 (1:200; BD Pharmingen), anti-TGF-β1 (1:200; Abcam), anti-Smad3 (1:200; Cell Signaling Technology), anti-F-actin (1:200; Solarbio), anti-COL1 (1:400; Proteintech), and anti-IL-10 (1:200; Abcam) primary antibodies for overnight at 4 °C. Next, the samples were incubated with FITC or Rhodamine-conjugated secondary antibodies for 1 h at room temperature (1:200; Invitrogen). After washing with PBS, the samples were mounted with mounting media containing 4',6-diamidino-2-phenyl-indole (DAPI) for nuclei staining and viewed by a Zeiss laser scanning confocal microscope LSM 710.

2.8. Statistical analysis

Values were averaged and expressed as mean \pm standard deviation. Statistical differences were evaluated by non-parameter analysis for AFM; For qPCR, Western blotting and semi-quantitative analysis of histological staining and micro-CT, and other experiments, Student's *t*-test (between two groups) and one-way ANOVA with the Tukey's multiple comparisons test (among three groups) were used by the SPSS 20.0 program. The differences were considered statistically significant at $\alpha = 0.05$.

3. Results and discussion

3.1. Fabrication and characterization of 3D mineralized cell microspheroids

Compared with commonly used MSCs (e.g., bone marrow-derived MSCs or periodontal ligament stem cells), DPSCs have excellent multi-lineage differentiation potential [16] and resistance to senescence; they can also be easily acquired from extracted teeth. Here, primary human DPSCs were isolated from dental pulp and characterized based on CD90⁺ CD105⁺ CD146⁺ CD29⁺ CD34⁻ CD11b⁻ markers, as reported previously (Fig. S1a). The isolated DPSCs exhibited osteogenic and adipogenic differentiation potentials, as indicated by positive alizarin red S and oil red O staining results (Fig. S1b).

To generate the 3D spheroid architecture, DPSCs were seeded into microporous agarose plates (Fig. 1a). Under 3D culture with regular medium, DPSCs could secrete abundant ECM and self-aggregate into uniform-sized soft CMs with a diameter of $120.31 \pm 8.12 \mu\text{m}$. When DPSCs were cultured in mineralizing culture medium containing poly-aspartic acid and calcium and phosphate ions, the self-produced ECM was mineralized, resulting in almost twofold greater size of solid MMCMs with a diameter of $218.75 \pm 7.65 \mu\text{m}$ (Fig. 1b). The enlarged size of MMCMs was due to the mineralization of ECM, which provided appropriate space between cells. Appropriate space provided by the extra dimension of cell microspheroids could maintain receptor

activation on the cell membrane [17]. Meanwhile, the cell phenotype and function may be regulated by changing the intrinsic stimuli or contents in the culture microenvironment of cell aggregates [18].

Biom mineralization of ECM endowed MMCMs distinct physiochemical properties compared to CMs. SEM showed that MMCMs exhibited a granular appearance, with inorganic mineral apatites (MAs) deposited around collagen filaments, while CMs showed a flat surface morphology with organic ECM alone (Fig. 1c, Fig. S2a, b). Cross-sectional examination demonstrated apatite aggregates deposited around DPSCs and ECM collagen filaments in MMCMs, while CMs had smooth morphology (Fig. 1c). AFM of MMCMs revealed an undulating topography with a greater amplitude and enhanced Young's modulus (420.8–1923.0 MPa), compared with CMs (311.0–720.0 MPa) (Fig. 1d, e). Two phases were observed in MMCMs: an inorganic phase with higher Young's modulus and an organic phase with lower Young's modulus. These results indicated that mineralization significantly increased the Young's modulus of ECM. Taken together, our findings indicated that endogenous ECM secreted by DPSCs exhibited distinct physiochemical properties in CMs and MMCMs, which may further influence cell activities in tissue engineering [19].

3.2. Promotion of DPSC viability by biom mineralization

Three-dimensional spheroid architecture assembled by cell-secreted ECM could provide an optimized microenvironment for stem cell accommodation, self-renewal, and multilineage differentiation potential [20,21]. Here, biom mineralized ECM with improved mechanical properties provided sufficient space and protection for internal cells to resist the stress from surrounding cells, thereby increasing cell viability (Fig. 2a). Cellular vulnerability to hypoxia places an important limitation on spheroid size. As CMs became larger, the inner cells were inevitably subjected to external pressure, which may result in exacerbated hypoxia. This was confirmed by Western blotting analysis of hypoxia markers HIF-1 α and CA IX (Fig. 2b). The expression levels of HIF-1 α and CA IX in CMs were nearly twofold greater than those in MMCMs on day 3, although no obvious hypoxia occurred on day 1.

Because of continuous insufficient nutrient substances and oxygen in central regions, the cell viability was decreased in the necrotic core [22]. To elucidate the cell fate of mineralized microspheroids, the mRNA expression patterns of apoptosis-related genes *BAX* and *BCL2* were examined (Fig. 2c). The expression level of the apoptosis-promoting gene *BAX* was significantly higher in CMs than in MMCMs on day 1, while the expression level of the apoptosis-suppressing gene *BCL2* was significantly lower in CMs than in MMCMs from day 1 to day 3. Furthermore, the higher expression level of cleaved Caspase3 protein in CMs indicated substantial cell apoptosis (Fig. 2d).

After 7 days of cultivation, > 99% of DPSCs in MMCMs were alive, while 18.26% \pm 0.90% DPSCs in CMs were dead after 7 days in culture (Fig. 2e). Notably, TEM scanning showed that the cells located in the core region in CMs were almost collapsed, indicating insufficient oxygen supply for internal cells (Fig. 2f). In contrast to CMs, the central cells in MMCMs showed normal cell morphology, with the presence of important organelles, including mitochondria, endoplasmic reticulum, Golgi apparatus and large quantities of secretory vesicles. ECM as an endogenous scaffold was reported to regulate function of stem cells [23]. The synthesis and secretion of extracellular vesicles (EVs) had intensive relationship with the autocrine and/or paracrine of stem cells and influenced the self-renewal and differentiation potential [24]. As previous studies reported, EVs showed therapeutic effects on tissue damage and induced tissue regeneration [25,26]. Taken together, these results demonstrated enhanced cell viability and active cellular function of MMCMs, which might possess better regeneration capacity *in vivo*.

3.3. Complete periodontal tissue regeneration by MMCMs

A successful tissue-engineered construct for complex periodontal

regeneration should possess adequate biomechanical stability to fill the defect space and prevent gingival epithelium migration; it should also deliver multiple cells (e.g., osteoblasts, fibroblasts, and cementoblasts) or recruit local progenitor stem cells toward bone and periodontal ligament tissues [27]. To evaluate the regeneration potential of MMCMs, a complete periodontal tissue defect including alveolar bone, periodontal ligament, and cementum loss was created at the buccal side of the distal buccal root of the mandibular first molar in rats (Fig. 3a) [13]. The defect area was filled with CMs or MMCMs and stabilized by covering with Bio-Gide® membrane (Geistlich). At 4 weeks postoperatively, the MMCM group reached 88.8% \pm 9.0% recovery with vertical bone augmentation of 3.55 \pm 0.36 mm, as determined on micro-CT cross-section images of the distal buccal root of the first molar (Fig. 3b). In marked contrast, the defect area showed almost no change in the control group with Bio-Gide® membrane alone. Semi-quantitative analysis of continuous scanning images of micro-CT showed that the bone volume density and trabecular number of the regenerated alveolar bone were much higher in the MMCM group than those in the CM and control groups.

The regeneration of alveolar bone is particularly important because bone tissue provides the most important structural basis for the stability of the tooth root, and is fundamental for the generation of Sharpey's fibers that are needed for the proper functioning of periodontal tissue [28]. Histological staining confirmed the complete periodontal tissue regeneration by MMCMs (Fig. 3c). The quantity of new bone area was significantly higher in the MMCM group than those in the CM and control groups. Native-like periodontium structures including alveolar bone, periodontal ligament, and cementum were formed in the MMCM group, while a mass of fibrous tissue alone was evident in the control group and limited neo-bone formation was observed in the CM group. Masson's trichrome staining and picrosirius red staining under polarized light were used to detect collagen formation in periodontal defects (Fig. 3d, e). Sparse, randomly arranged collagen fibers were formed in the control and CM groups. In marked contrast, dense hierarchically organized collagen fibers were regenerated by MMCMs and acted as functional periodontal ligament to connect newly formed alveolar bone with cementum [29].

Construction of a microenvironment similar to typical physiological conditions is a key factor for the regeneration of complex periodontal tissues. Here, immunofluorescence staining demonstrated that the recruited cells in defect area expressed both CD90 and CD73 (surface markers for rat MSCs) at 4 weeks postoperatively (Fig. 3f). The number of CD90⁺CD73⁺ cells was significantly greater in the MMCM group than those in the CM and control groups. BMP2, an important factor during bone formation, was highly expressed in and around the newly formed bone in the MMCM group; additionally, POSTN, a vital component of native periodontal ligament, was highly expressed in newly formed periodontal ligament tissues in the MMCM group (Fig. S3). These results indicated that MMCMs may induce appropriate microenvironment for stem cells differentiation to form bone and fibrous tissue in periodontal defect area.

To clarify the possible signaling pathway involved in the MMCM-induced periodontal regeneration, we testified the expression level of TGF- β 1, an important marker of active matrix metabolism [30], and found the enhanced expression of TGF- β 1 both in neo-bone and periodontal ligament area in the MMCM group (Fig. 3g). TGF- β 1 was reported to be loaded on different scaffolds in tissue engineering strategy and induced multiple types of tissue regeneration [31,32]. Taken together, these observations indicated that MMCMs provide a favorable microenvironment to promote complete periodontal tissue formation, and that TGF- β 1 may play an important role in this process.

3.4. Promotion of ECM synthesis and osteogenesis in MMCMs by activating the TGF- β 1/Smad3 signaling pathway

To elucidate the TGF- β 1 signaling pathway related mechanism in

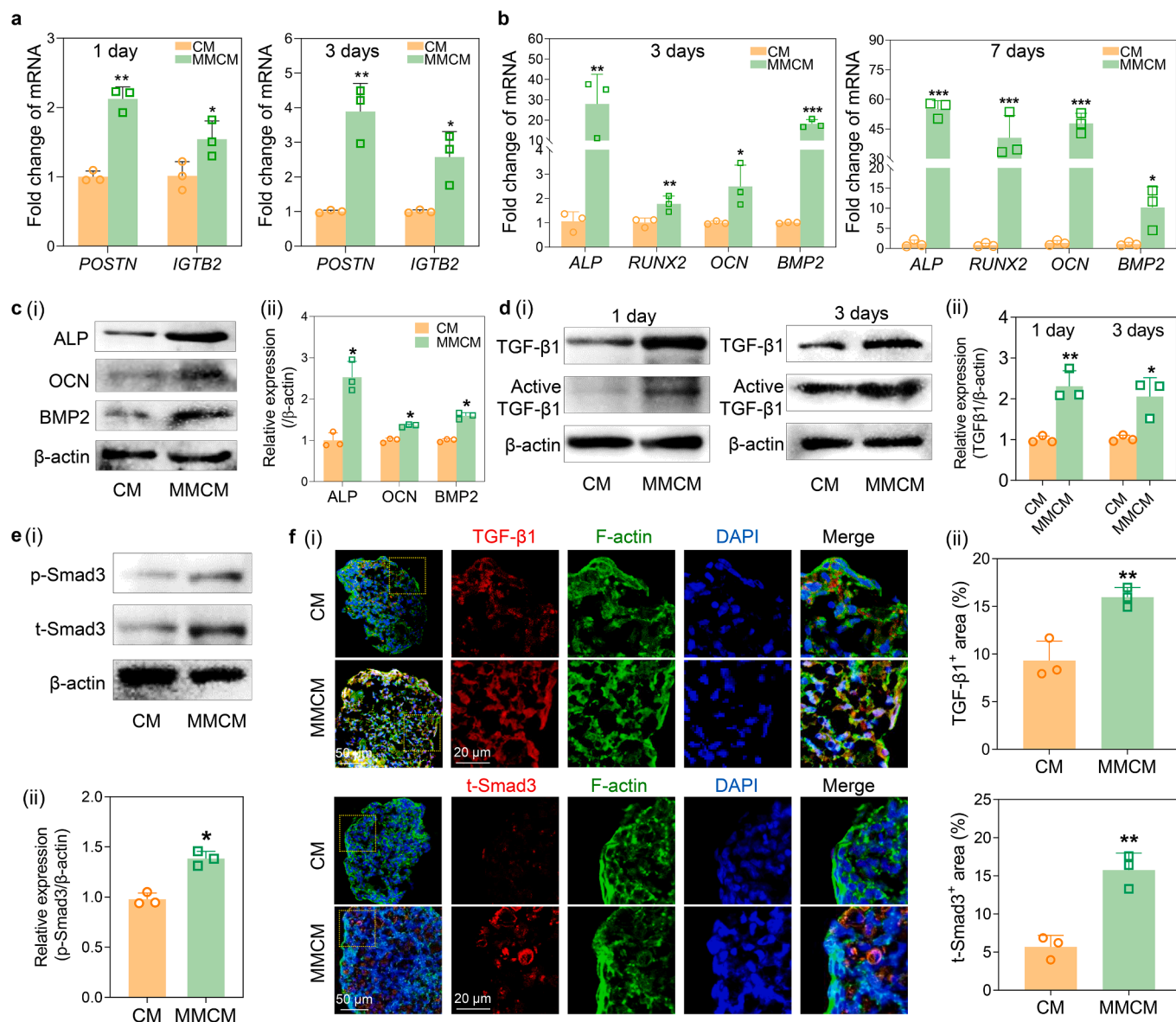


Fig. 4. Promotion of ECM synthesis and osteogenesis and activation of TGF- β 1/Smad3 signaling pathway by MMCs. (a) *POSTN* and *IGTB2* gene expression on day 1 and day 3 by qPCR ($n = 3$). (b) *ALP*, *RUNX2*, *OCN* and *BMP2* gene expression on day 3 and day 7 by qPCR ($n = 3$). (c) Western blotting (i) and semi-quantitative analysis (ii) of *ALP*, *OCN* and *BMP2* on day 7 in CMs and MMCs ($n = 3$). (d) Western blotting (i) and semi-quantitative analysis (ii) of TGF- β 1 in CMs and MMCs ($n = 3$). (e) Western blotting (i) and semi-quantitative analysis (ii) of p-Smad3 and Smad3 in CMs and MMCs on day 1 ($n = 3$). (f) Immunofluorescence staining (i) and semi-quantitative analysis (ii) of TGF- β 1, Smad3 and F-actin in CMs and MMCs on day 3 ($n = 3$). The P values were calculated by Student's t -test. *: $P < 0.05$, **: $P < 0.01$, ***: $P < 0.001$.

ECM synthesis and osteogenesis in MMCs, we firstly testified the expression of ECM-related genes *POSTN* and *ITGB2*—both critical in cell adhesion, differentiation, and periodontal regeneration [33]—in CMs and MMCs. The results showed that *POSTN* and *ITGB2* were highly expressed in MMCs, indicating that biomineralization promotes endogenous ECM synthesis and secretion (Fig. 4a). The osteogenic capacity of MMCs was activated with enhanced expression levels of osteogenesis-related markers *ALP*, *RUNX2*, *OCN* and *BMP2*. In particular, the expression levels of *ALP* and *OCN* increased sharply from day 3 to day 7 (Fig. 4b). Accordingly, the expression of *ALP*, *OCN* and *BMP2* was tested by Western blotting and showed consistent tendency with the results of qPCR (Fig. 4c).

The expression of TGF- β 1 was also examined in CMs and MMCs. Western blotting analysis showed that ECM mineralization promoted the expression and activation of TGF- β 1 from the early stages during the cultivation process from day 1 to day 3 (Fig. 4d). The phosphorylation

and expression of Smad3, downstream of the TGF- β 1 signaling pathway, were also elevated at early stages in MMCs (Fig. 4e). Immunofluorescence staining confirmed the activation of TGF- β 1/Smad3 in MMCs (Fig. 4f). These observations suggested that under conditions of biomineralization, TGF- β 1/Smad3 signaling pathway was activated and might affect the activation of downstream ECM synthesis and osteogenesis.

To confirm the functional role of TGF- β 1/Smad3 signaling pathway, we used a selective TGF- β 1 inhibitor, LY364947 [34]. Gross morphological observations showed that TGF- β 1 inhibition did not change the size of MMCs but decreased the homogeneity and ECM secretion at high magnification; immunofluorescence staining demonstrated the downregulation of COL1 (Fig. 5a). The shrinkage of the cytoskeleton was observed after 3 days of cultivation. The morphological changes indicated that the TGF- β 1/Smad3 signaling pathway participates in cytoskeletal arrangement [35], which may further influence stem cell

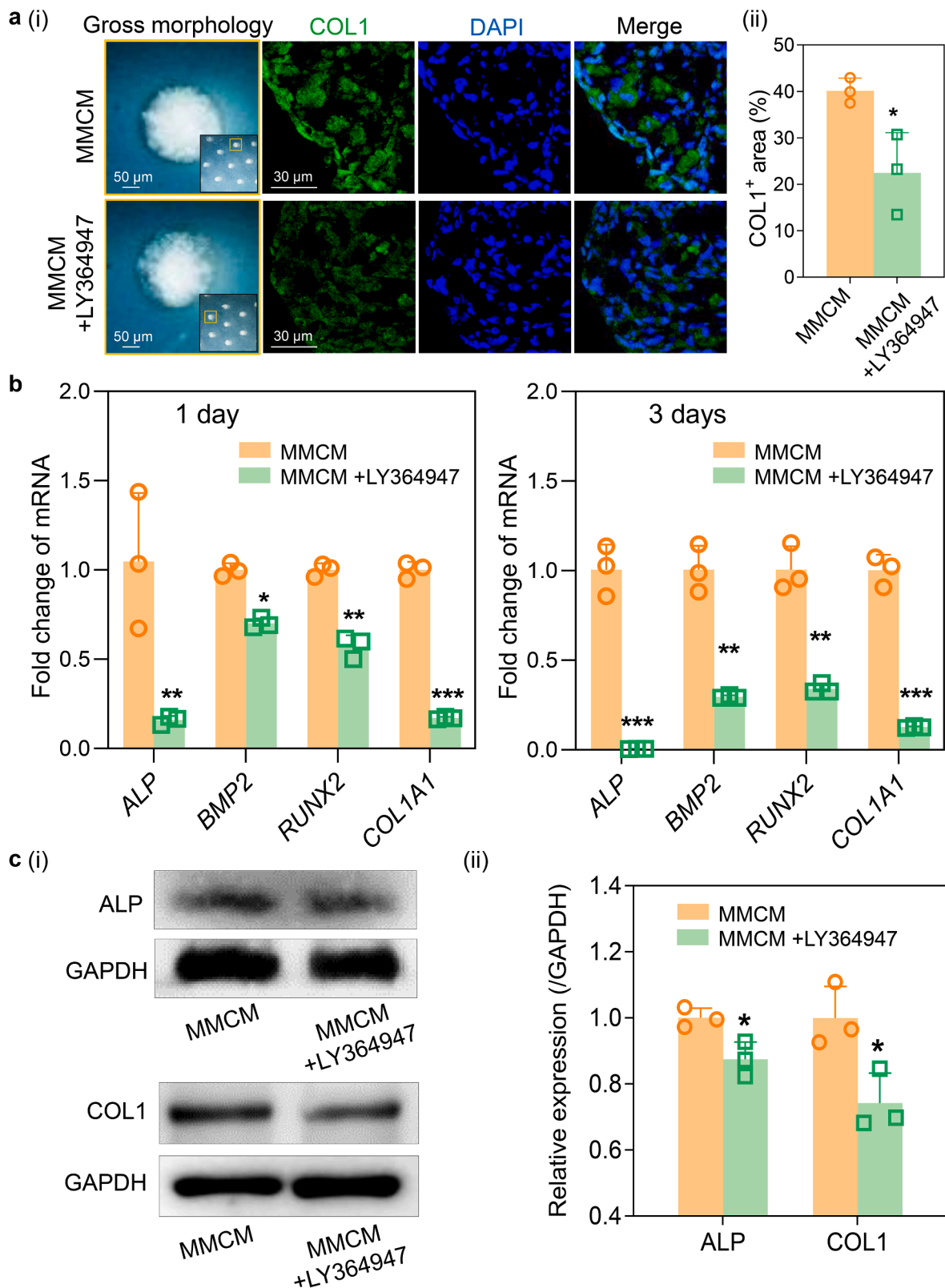


Fig. 5. Impaired osteogenesis and ECM synthesis in MMCMs by blocking TGF- β 1/Smad3 signaling pathway. **(a) (i)** Gross morphology and COL1 immunofluorescence staining of MMCMs and MMCMs treated with LY364947 for 3 days. **(ii)** Semi-quantitative analysis of COL1⁺ area in the MMCM and MMCM + LY364947 groups ($n = 3$). **(b)** Downregulated gene expression of *ALP*, *BMP2*, *RUNX2* and *COL1A1* by the inhibition of TGF- β 1/Smad3 signaling pathway ($n = 3$). **(c)** Western blotting **(i)** and semi-quantitative analysis **(ii)** showing downregulated expression of ALP and COL1 by the administration of LY364947 for 3 days ($n = 3$). The P values were calculated by Student's t -test. *: $P < 0.05$, **: $P < 0.01$, ***: $P < 0.001$.

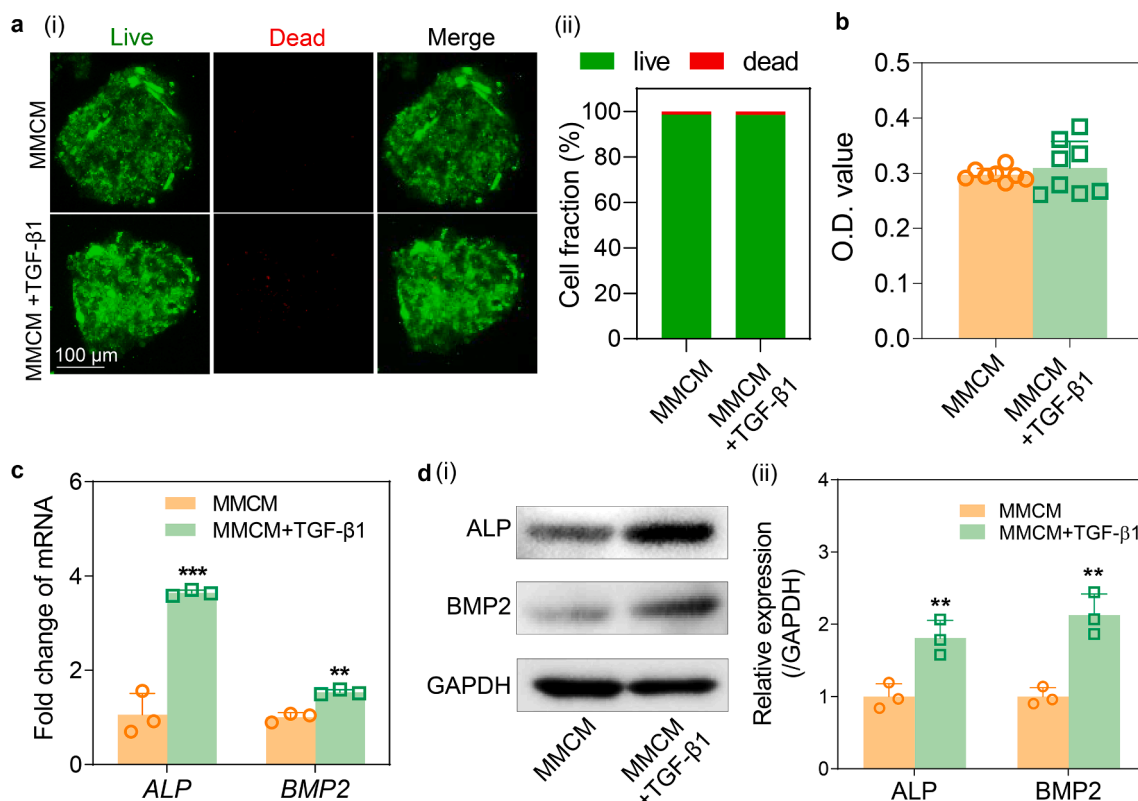


Fig. 6. Promotion of osteogenesis in MMCs under exogenous TGF- β 1 stimulation. (a) Live/dead assay on day 7 (i) and its semi-quantitative analysis (ii). (b) CCK-8 analysis of MMCs and MMCs treated with TGF- β 1 on day 7 ($n = 8$). (c) Upregulated gene expression of *ALP* and *BMP2* by the administration of TGF- β 1 on day 7 ($n = 3$). (d) Western blotting (i) and semi-quantitative analysis (ii) showing upregulated expression of *ALP* and *BMP2* by the administration of TGF- β 1 on day 7 ($n = 3$). The P values were calculated by Student's t -test. **: $P < 0.01$, ***: $P < 0.001$.

function. This hypothesis was confirmed by the significantly down-regulated gene expression of the osteogenic markers *ALP*, *BMP2*, *RUNX2*, and ECM-related marker *COL1A1* in the MMCM + LY364947 group (Fig. 5b). Meanwhile, the expression levels of *ALP* and *COL1* were tested by Western blotting and showed consistent tendency with the results of qPCR (Fig. 5c). These results demonstrated that TGF- β 1 signaling pathway positively regulated ECM synthesis and secretion in MMCs [36]. The effects of TGF- β 1 signaling pathway activation on osteogenesis remain controversial. Previous studies have suggested that the activation of TGF- β 1 signaling pathway inhibited osteogenic differentiation in bone marrow derived MSCs [37]. In contrast, Manokawinchoke *et al.* showed that the activation of TGF- β 1 signaling could induce upregulation of osteogenesis-related genes in periodontal ligament cells [38]. These opposite results might be due to various exogenous stimulus, distinct derivation of cells, and different stage of osteogenesis.

3.5. Enhanced periodontal tissue regeneration using MMCs loaded with TGF- β 1

To test whether TGF- β 1 could improve the regenerative potential of MMCs, TGF- β 1 was delivered into the culture medium of MMCs for 7 days. Live/dead and CCK-8 assays showed that exogenous TGF- β 1 stimulation did not influence cell viability after cultivation for 7 days (Fig. 6a, b). Consistent with our previous findings, the MMCM + TGF- β 1 group showed enhanced osteogenesis related markers, *ALP* and *BMP2*, compared with the MMCM group (Fig. 6c, d).

To examine how TGF- β 1-treated MMCs exerts biological effects *in vivo*, MMCs or MMCs with TGF- β 1 were implanted into full periodontal defect areas. After implantation for 2 weeks, continuous alveolar bone with higher density was formed in the defect area in the

MMCM + TGF- β 1 group (Fig. 7a). Quantitative analysis revealed that the bone volume and trabecular bone of the defect area were significantly enhanced in the MMCM + TGF- β 1 group, compared with the MMCM group. The microstructure of newly formed periodontal tissues was assessed by HE, Masson's trichrome, and picrosirius red staining; the results indicated that TGF- β 1 promoted the formation of alveolar bone and functional, mature, well-organized periodontal fibers (Fig. 7b-d). SEM confirmed that dense, hierarchically organized periodontal fibers were inserted into the newly formed alveolar bone and cementum in the MMCM + TGF- β 1 group, with periodic banding of collagen microfibrils visible under high magnification (Fig. 7e). Furthermore, endogenous MSC recruitment was detected by immunofluorescence analysis at 2 weeks postoperatively. In the MMCM + TGF- β 1 group, more CD73⁺CD90⁺ MSCs were recruited into the defect area (Fig. 7f). Meanwhile, an important anti-inflammatory cytokine interleukin-10, which plays a critical role in organ repair and cementoblastic differentiation [39], was highly expressed on the surface of root and alveolar bone in the MMCM + TGF- β 1 group, suggesting TGF- β 1-treated MMCs could accelerate bone and cementum regeneration (Fig. S4). Taken together, consistent with the results of *in vitro* studies, the *in vivo* observations suggested that TGF- β 1 could boost MMCM-induced periodontal tissue regeneration by promoting MSC recruitment.

Owing to the complex structure of periodontium, different cytokines have been applied to enhance periodontal regeneration, including FGF-2 for fiber synthesis [40] and IL-2 for immunoregulation [41]. Moreover, the clinical periodontal defects are often accompanied with local infection and sustained inflammatory infiltration, which may interfere with the function of implanted MSC aggregates. Whether the combination of TGF- β 1 with other type of cytokines or bioactive molecules could improve the regenerative effects of MMCs in inflammatory or infectious condition still need further investigation.

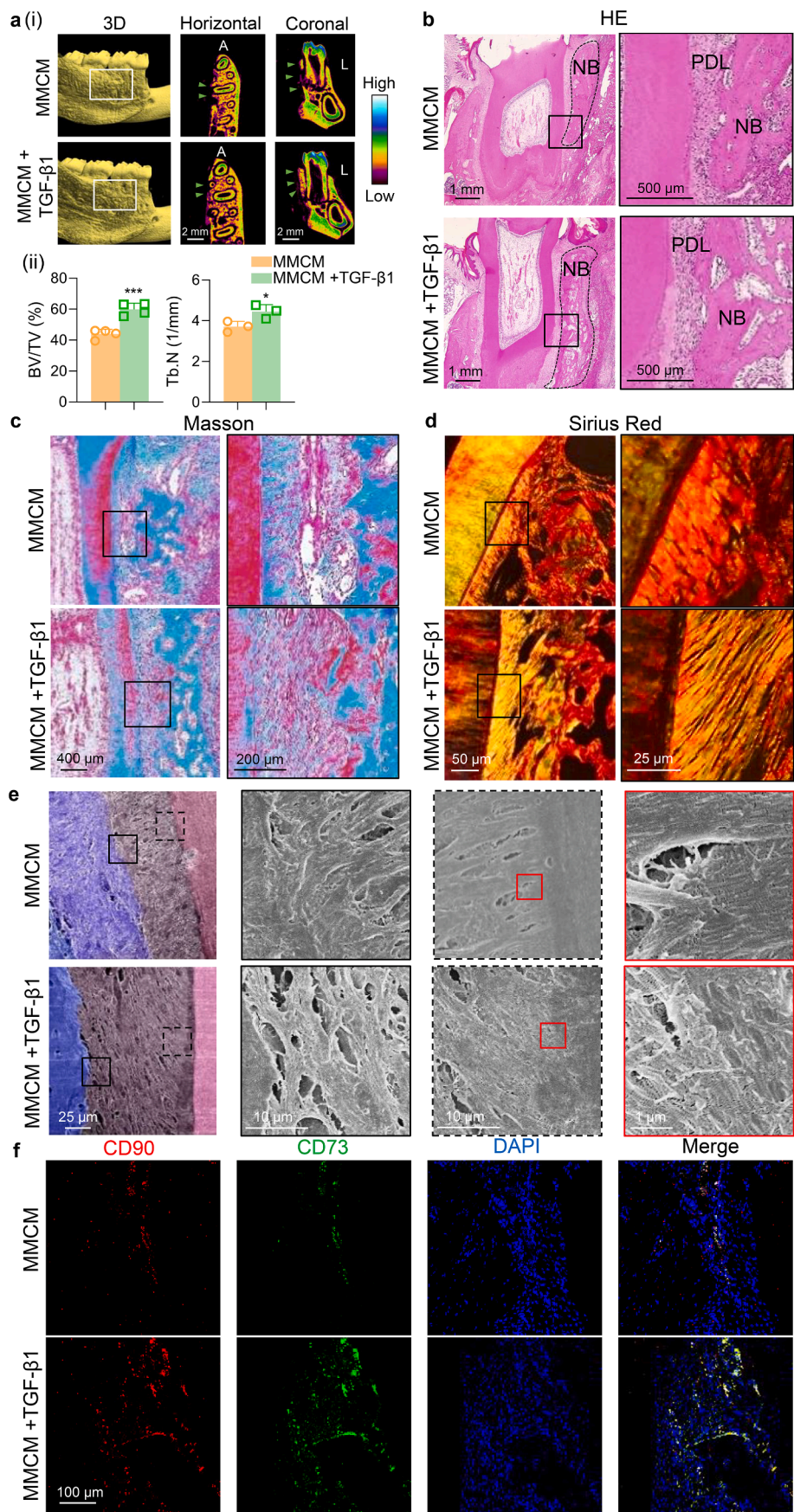


Fig. 7. Enhanced periodontal tissue regeneration using MMCMs loaded with TGF-β1. **(a) (i)** Representative micro-CT images (3D, horizontal plane, coronal plane) of periodontal tissues at 2 weeks post-operatively. A: anterior; L: lingual; white arrows: newly formed bone. **(ii)** Semi-quantitative analysis of bone-related parameters including Tb.N and BV/TV% ($n = 3$ or 4). The P values were calculated by Student's t -test. *: $P < 0.05$, ***: $P < 0.001$. **(b-d)** HE, Masson trichrome and picrosirius red (under polarized light) stainings of coronal sections. NB: new bone; PDL: periodontal ligament; Black dotted frame: the boundary of alveolar bone area; black frame: high magnification the defect area. **(e)** Representative SEM images of newly formed periodontal tissues. Pink part: root; gray part: periodontal ligament; blue part: alveolar bone; violet part: transition area. The black/red frame represented the location of magnified images. **(f)** Representative images of immunofluorescence staining of CD90 (red) and CD73 (green). (For interpretation of the references to colour in this figure legend, the reader is referred to the web version of this article.)

4. Conclusion

This study demonstrated complete periodontal tissue regeneration by mineralized microspheroids and revealed the underlying mechanisms. We showed the mineralized microspheroids exhibited enhanced strength, provided sufficient oxygen supply and avoided the development of a central necrotic core. ECM mineralization increased cell viability, ECM secretion, and osteogenesis via the TGF- β 1/Smad3 signaling pathway. These enhancing effects could be blocked by TGF- β 1 depletion. MMCM-induced improvement of ECM secretion and osteogenic differentiation promoted the complete regeneration of periodontal tissues, including alveolar bone, periodontal ligament, and cementum, through activation of the TGF- β 1/Smad3 signaling pathway. This study demonstrated that mineralized microspheroids have potential for use in stem cell therapy to facilitate clinical periodontal tissue regeneration.

Declaration of competing interest

The authors declare that they have no known competing financial interests or personal relationships that could have appeared to influence the work reported in this paper.

Acknowledgements

This work was supported by the National Natural Science Foundations of China (81871492 and 81901053), Ten-Thousand Talents Program (QNB2019-2), Key R & D Plan of Ningxia Hui Autonomous Region (2020BCG01001), China Postdoctoral Science Foundation (2020M680263), Postdoctoral Fellowship of Peking-Tsinghua Center for Life Sciences (2020) and Peking University Medicine Fund of Fostering Young Scholars' Scientific & Technological Innovation and the Fundamental Research Funds for the Central Universities (BMU2018PYB017). Dr. S.J. Cui and Dr. Y. Fu contributed equally to this work.

Appendix A. Supplementary data

Supplementary data to this article can be found online at <https://doi.org/10.1016/j.cej.2021.133220>.

References

- [1] B.L. Pihlstrom, B.S. Michalowicz, N.W. Johnson, Periodontal diseases, *Lancet* 366 (9499) (2005) 1809–1820.
- [2] F.-M. Chen, J. Zhang, M. Zhang, Y. An, F. Chen, Z.-F. Wu, A review on endogenous regenerative technology in periodontal regenerative medicine, *Biomaterials* 31 (31) (2010) 7892–7927.
- [3] P.M. Bartold, S. Gronthos, S. Ivanovski, A. Fisher, D.W. Huttmacher, Tissue engineered periodontal products, *J Periodontol Res* 51 (1) (2016) 1–15.
- [4] C.H. Park, H.F. Rios, Q. Jin, J.V. Sugai, M. Padial-Molina, A.D. Taut, C.L. Flanagan, S.J. Hollister, W.V. Giannobile, Tissue engineering bone-ligament complexes using fiber-guiding scaffolds, *Biomaterials* 33 (1) (2012) 137–145.
- [5] Y.S. Liu, T. Zhang, M. Li, Z.G. Ouyang, F. Gao, C.Y. Liu, C. Li, D.Y. Liu, Z.M. Zhou, PLGA hybrid porous microspheres as human periodontal ligament stem cell delivery carriers for periodontal regeneration, *Chem Eng J* 420 (2021), 129703.
- [6] K. Lin, W. Yuan, L. Wang, J. Lu, L. Chen, Z. Wang, J. Chang, Evaluation of host inflammatory responses of beta-tricalcium phosphate bioceramics caused by calcium pyrophosphate impurity using a subcutaneous model, *J Biomed Mater Res B Appl Biomater* 99 (2) (2011) 350–358.
- [7] C. Fu, D. Luo, M. Yu, N. Jiang, D. Liu, D. He, Y. Fu, T. Zhang, Y. Qiao, Y. Zhou, Y. Liu, Embryonic-like mineralized extracellular matrix/stem cell microspheroids as a bone graft substitute, *Adv Healthc Mater* 7 (19) (2018) 1800705, <https://doi.org/10.1002/adhm.v7.1910.1002/adhm.201800705>.
- [8] K.-R. Yu, S.-R. Yang, J.-W. Jung, H. Kim, K. Ko, D.W. Han, S.-B. Park, S.W. Choi, S.-K. Kang, H. Schöler, K.-S. Kang, CD49f enhances multipotency and maintains stemness through the direct regulation of OCT4 and SOX2, *Stem Cells* 30 (5) (2012) 876–887.
- [9] A. Shakouri-Motlagh, A.J. O'Connor, S.P. Brennecke, B. Kalionis, D.E. Heath, Native and solubilized decellularized extracellular matrix: a critical assessment of their potential for improving the expansion of mesenchymal stem cells, *Acta Biomater* 55 (2017) 1–12.
- [10] E. Fennema, N. Rivron, J. Rouwkema, C. van Blitterswijk, J. de Boer, Spheroid culture as a tool for creating 3D complex tissues, *Trends Biotechnol* 31 (2) (2013) 108–115.

- [11] J.J. Bara, R.G. Richards, M. Alini, M.J. Stoddart, Concise review: Bone marrow-derived mesenchymal stem cells change phenotype following in vitro culture: implications for basic research and the clinic, *Stem Cells* 32 (7) (2014) 1713–1723.
- [12] H. Zhang, S. Liu, B. Zhu, Q. Xu, Y. Ding, Y. Jin, Composite cell sheet for periodontal regeneration: crosstalk between different types of MSCs in cell sheet facilitates complex periodontal-like tissue regeneration, *Stem Cell Res Ther* 7 (1) (2016) 168.
- [13] C. Vaquette, S. Saifzadeh, A. Farag, D.W. Huttmacher, S. Ivanovski, Periodontal tissue engineering with a multiphasic construct and cell sheets, *J Dent Res* 98 (6) (2019) 673–681.
- [14] Z. Jiang, N. Li, D. Zhu, L. Ren, Q. Shao, K. Yu, G. Yang, Genetically modified cell sheets in regenerative medicine and tissue engineering, *Biomaterials* 275 (2021), 120908.
- [15] C.S. Ong, X. Zhou, J. Han, C.Y. Huang, A. Nashed, S. Khatri, G. Mattson, T. Fukunishi, H. Zhang, N. Hibino, In vivo therapeutic applications of cell spheroids, *Biotechnol Adv* 36 (2) (2018) 494–505.
- [16] S. Gronthos, M. Mankani, J. Brahmi, P.G. Robey, S. Shi, Postnatal human dental pulp stem cells (DPSCs) in vitro and in vivo, *Proc Natl Acad Sci U S A* 97 (25) (2000) 13625–13630.
- [17] M.W. Laschke, M.D. Menger, Spheroids as vascularization units: from angiogenesis research to tissue engineering applications, *Biotechnology Advances* 35 (6) (2017) 782–791.
- [18] Z.H. Syedain, L.A. Meier, J.W. Bjork, A. Lee, R.T. Tranquillo, Implantable arterial grafts from human fibroblasts and fibrin using a multi-graft pulsed flow-stretch bioreactor with noninvasive strength monitoring, *Biomaterials* 32 (3) (2011) 714–722.
- [19] F.-M. Chen, X. Liu, Advancing biomaterials of human origin for tissue engineering, *Prog Polym Sci* 53 (2016) 86–168.
- [20] H. Chen, H. Fu, X. Wu, Y. Duan, S. Zhang, H. Hu, Y. Liao, T. Wang, Y. Yang, G. Chen, Z. Li, W. Tian, Regeneration of pulpo-dentinal-like complex by a group of unique multipotent CD24a(+) stem cells, *Sci Adv* 6 (15) (2020) eaay1514.
- [21] N. Gjorevski, N. Sachs, A. Manfrin, S. Giger, M.E. Bragina, P. Ordóñez-Morán, H. Clevers, M.P. Lutolf, Designer matrices for intestinal stem cell and organoid culture, *Nature* 539 (7630) (2016) 560–564.
- [22] K. Alessandri, B.R. Sarangi, V.V. Gurchenkov, B. Sinha, T.R. Kiessling, L. Fetler, F. Rico, S. Scheuring, C. Lamaze, A. Simon, S. Geraldo, D. Vignjevic, H. Domejean, L. Rolland, A. Funfak, J. Bibette, N. Bremond, P. Nassoy, Cellular capsules as a tool for multicellular spheroid production and for investigating the mechanics of tumor progression in vitro, *Proc Natl Acad Sci U S A* 110 (37) (2013) 14843–14848.
- [23] F. Shang, L. Ming, Z. Zhou, Y. Yu, J. Sun, Y. Ding, Y. Jin, The effect of licochalcone A on cell-aggregates ECM secretion and osteogenic differentiation during bone formation in metaphyseal defects in ovariectomized rats, *Biomaterials* 35 (9) (2014) 2789–2797.
- [24] C. Balbi, M. Piccoli, L. Barile, A. Papait, A. Armirotti, E. Principi, D. Reverberi, L. Pascucci, P. Becherini, L. Varesio, M. Moggi, D. Coviello, T. Bandiera, M. Pozzobon, R. Cancedda, S. Bollini, First characterization of human amniotic fluid stem cell extracellular vesicles as a powerful paracrine tool endowed with regenerative potential, *Stem Cells Transl Med* 6 (5) (2017) 1340–1355.
- [25] A. Psaraki, L. Ntari, C. Karakostas, D. Korrou-Karava, M.G. Roubelakis, Extracellular vesicles derived from mesenchymal stem/stromal Cells: the regenerative impact in liver diseases, *Hepatology* (2021).
- [26] R.C. de Abreu, H. Fernandes, P.A. da Costa Martins, S. Sahoo, C. Emanuelli, L. Ferreira, Native and bioengineered extracellular vesicles for cardiovascular therapeutics, *Nat Rev Cardiol* 17 (11) (2020) 685–697.
- [27] M.M. Hasani-Sadrabadi, P. Sarrion, N. Nakatsuka, T.D. Young, N. Taghdiri, S. Ansari, T. Aghaloo, S. Li, A. Khademosseini, P.S. Weiss, A. Moshaverinia, Hierarchically patterned polydopamine-containing membranes for periodontal tissue engineering, *ACS Nano* 13 (4) (2019) 3830–3838.
- [28] Y. Liang, Z. Hu, B. Chang, X. Liu, Quantitative characterizations of the Sharpey's fibers of rat molars, *J Periodontol Res* 55 (2) (2020) 307–314.
- [29] C.H. Park, J.H. Oh, H.M. Jung, Y. Choi, S.U. Rahman, S. Kim, T.I. Kim, H.I. Shin, Y. S. Lee, F.H. Yu, J.H. Baek, H.M. Ryoo, K.M. Woo, Effects of the incorporation of epsilon-aminocaproic acid/chitosan particles to fibrin on cementoblast differentiation and cementum regeneration, *Acta Biomater* 61 (2017) 134–143.
- [30] L. Feng, R. Yang, D. Liu, X. Wang, Y. Song, H. Cao, D. He, Y. Gan, X. Kou, Y. Zhou, PDL progenitor-mediated PDL recovery contributes to orthodontic relapse, *J Dent Res* 95 (9) (2016) 1049–1056.
- [31] G. Cheng, J.H. Dai, J.W. Dai, H. Wang, S. Chen, Y.H. Liu, X.Y. Liu, X.R. Li, X. Zhou, H.B. Deng, Z. Li, Extracellular matrix imitation utilizing nanofibers-embedded biomimetic scaffolds for facilitating cartilage regeneration, *Chem Eng J* 410 (2021), 128379.
- [32] B. Zhang, Q. Luo, B. Deng, Y. Morita, Y. Ju, G. Song, Construction of tendon replacement tissue based on collagen sponge and mesenchymal stem cells by coupled mechano-chemical induction and evaluation of its tendon repair abilities, *Acta Biomaterialia* 74 (2018) 247–259.
- [33] H.N. Tang, Y. Xia, Y. Yu, R.X. Wu, L.N. Gao, F.M. Chen, Stem cells derived from “inflamed” and healthy periodontal ligament tissues and their sheet functionalities: a patient-matched comparison, *J Clin Periodontol* 43 (1) (2016) 72–84.
- [34] Z.Q. Zuo, K.G. Chen, X.Y. Yu, G. Zhao, S. Shen, Z.T. Cao, Y.L. Luo, Y.C. Wang, J. Wang, Promoting tumor penetration of nanoparticles for cancer stem cell therapy by TGF-beta signaling pathway inhibition, *Biomaterials* 82 (2016) 48–59.
- [35] X. Dong, B. Zhao, R.E. Jacob, J. Zhu, A.C. Koksals, C. Lu, J.R. Engen, T.A. Springer, Force interacts with macromolecular structure in activation of TGF-beta, *Nature* 542 (7639) (2017) 55–59.
- [36] M. Yu, D. Luo, J. Qiao, J. Guo, D. He, S. Jin, L. Tang, Y.U. Wang, X. Shi, J. Mao, S. Cui, Y.U. Fu, Z. Li, D. Liu, T. Zhang, C. Zhang, Z. Li, Y. Zhou, Y. Liu,

- A hierarchical bilayer architecture for complex tissue regeneration, *Bioactive Materials* (2021), <https://doi.org/10.1016/j.bioactmat.2021.08.024>.
- [37] Y. Huang, Y. Zheng, L. Jia, W. Li, Long noncoding RNA H19 promotes osteoblast differentiation via TGF-beta1/Smad3/HDAC signaling pathway by deriving miR-675, *Stem Cells* 33 (12) (2015) 3481–3492.
- [38] J. Manokawinchoke, P. Pavasant, C. Sawangmake, N. Limjeerajarus, C. N. Limjeerajarus, H. Egusa, T. Osathanon, Intermittent compressive force promotes osteogenic differentiation in human periodontal ligament cells by regulating the transforming growth factor-beta pathway, *Cell Death Dis* 10 (10) (2019) 761.
- [39] Xuan Li, Xiao-Tao He, De-Qin Kong, Xin-Yue Xu, Rui-Xin Wu, Li-Juan Sun, Bei-Min Tian, Fa-Ming Chen, M2 Macrophages Enhance the Cementoblastic Differentiation of Periodontal Ligament Stem Cells via the Akt and JNK Pathways, *Stem Cells* 37 (12) (2019) 1567–1580.
- [40] D.L. Cochran, T.J. Oh, M.P. Mills, D.S. Clem, P.K. McClain, R.A. Schallhorn, M. K. McGuire, E.T. Scheyer, W.V. Giannobile, M.S. Reddy, R.V. Abou-Arrej, P. J. Vassilopoulos, R.J. Genco, N.C. Geurs, A. Takemura, A randomized clinical trial evaluating rh-FGF-2/beta-TCP in periodontal defects, *J Dent Res* 95 (5) (2016) 523–530.
- [41] Z. Liu, X. Chen, Z. Zhang, X. Zhang, L. Saunders, Y. Zhou, P.X. Ma, Nanofibrous spongy microspheres to distinctly release miRNA and growth factors to enrich regulatory T cells and rescue periodontal bone loss, *ACS Nano* 12 (10) (2018) 9785–9799.